Preprint
UCRL-JC-136032

The Partitioning of Uranium and Neptunium onto Hydrothermally Altered Concrete

P. Zhao, P.G. Allen, E.R. Sylwester, B.E. Viani

This article was submitted to
7th International Conference in the Chemistry and Migration Behavior of Actinides and Fission Products in the Geosphere, Lake Tahoe, NV, September 26-October 1, 1999

October 14, 1999

U.S. Department of Energy

Lawrence
Livermore
National
Laboratory

THE PARTITIONING OF URANIUM AND NEPTUNIUM ONTO HYDROTHERMALLY ALTERED CONCRETE

By P. Zhao[1], P. G. Allen[1], E. R. Sylwester[1], and B. E. Viani[2*]

[1]G. T. Seaborg Institute for Transactinium Science
[2]Geosciences & Environmental Technologies Division
Lawrence Livermore National Laboratory, Livermore, California 94550, USA

Uranium(VI)/Neptunium(V)/Sorption/Cementitious materials/Carbonate complexation/colloid/EXAFS

Summary

Partition coefficients (K_d) of U(VI) and Np(V) on untreated and hydrothermally altered concrete were measured in 0.01 M NaCl and 0.01 M $NaHCO_3$ solutions as functions of concentration of the radionuclides, pH, and time. The partition coefficients for both U(VI) and Np(V) on hydrothermally altered concrete are significantly lower than those on untreated concrete. The partition of both U(VI) and Np(V) are pH dependent, although the pH dependence does not necessarily reflect precipitation of U and Np-bearing phases. Both sorption and precipitation appear to control partitioning of U to concrete; sorption alone appears to control partition of Np to concrete. The presence of 0.01 M carbonate species in solution decreases K_d of U(VI) for both treated and untreated concrete to a similar value of ~500 mL/g indicating a significant impact on U(VI) sorption. However, the presence of carbonate only reduced the K_d of Np(V) by one order of magnitude or less. Our results also show that significant amounts of uranium and neptunium in aqueous phase are associated with suspended colloids. In most cases, the colloid-associated uranium and neptunium are the predominant species in the liquid phase. X-ray absorption spectroscopy

---

* Authors to whom correspondence should be addressed.

analysis of U/concrete mixtures at different pHs and times indicate that uranyl ions are partitioned as monomeric species on untreated concrete, but oligomeric species on hydrothermally altered concrete. Similar analysis of Np/concrete mixtures shows that about half of the partitioned Np(V) is reduced to Np(IV) over a period of 6 months.

Introduction

Cementitious materials that are used to construct the ground support for high-level repositories have a high probability of interacting with radionuclide-bearing fluids derived from failed waste packages. Cementitious materials provide a highly alkaline environment; pore fluids in concrete can have pH>10 for thousands to hundreds of thousands of years [1]. Studies have shown that fresh concrete and cement phases strongly retard or immobilize certain actinides [2, 3]. Consequently, cementitious materials may serve as a barrier to the release of the radionuclides to the far field. However, the effect of thermal alteration of these materials, which may occur in high-level repositories, on their interaction with radionuclides has not been addressed. In contrast to retardation, colloidal silica-enriched particles that are abundant in the pore fluids of cementitious materials may facilitate radionuclide migration through the near-field into the adjacent geological environment [4]. Due to the uncertainties of these two opposite effects, it is important to investigate the interaction of actinides with cementitious materials under varying conditions.

It is expected that cementitious materials in high-level waste repositories will be subjected to and altered by hot dry and/or humid conditions for hundreds to thousands of years by the time they interact with radionuclide-bearing fluids. After alteration, the chemical and mineralogical proper-

ties of these materials will be significantly different from that of the as-placed or fresh concrete. To assess the effect that this alteration would have on radionuclide interactions, samples of hardened concrete (untreated concrete) were hydrothermally heated at 200 °C for 8 months (treated concrete). The concrete used in the experiments consisted of portland cement with an aggregate of dolomitic limestone. X-ray diffraction analysis has shown that portlandite and amorphous calcium silicate hydrate gels were converted to the crystalline calcium silicate hydrate minerals tobermorite (11①), xonotlite, and scawtite, and clay minerals by the hydrothermal treatment. Calcite, dolomite, and quartz in the aggregate were unchanged by the treatment.

This paper presents the results of batch experiments to obtain partition coefficients (K_d) for U(VI) and Np(V) on untreated and treated concrete in 0.01 M NaCl and 0.01 M$NaHCO_3$ solutions as functions of the concentration of the radionuclides, pH and time.

Experimental

Reagents and Equipment – The reagents used were A.R. grade. The DI water used was made from a Millipore Milli-Q™ water system. The stock solutions of U(VI) and Np(V) were in 1 M HCl and 2 M $HClO_4$, respectively. The oxidation states of U(VI) and Np(V) in the stock solutions were confirmed using UV/VIS spectrometry. Isotopes ^{233}U and ^{237}Np were used as tracers for nuclear counting. A Tri-Carb 2500 Liquid Scintillation analyzer from Packard Instrument Company was used for α-liquid scintillation counting (LSC) and α,β-LSC for U and Np aqueous samples, respectively. The α,β-LSC results for ^{237}Np were verified using its γ-ray at 29.4 keV detected with a high purity germanium detector.

Partition Experiment – Samples of crushed (<53 μm) treated and untreated concrete were reacted with 0.01 M NaCl containing U and Np at mass/volume ratio of 0.4 g/L at room temperature (23±2 °C). Filtered and unfiltered samples of the aqueous phase were taken as a function of time to assess soluble radionuclides, as well as radionuclides that associated with suspended colloidal particles. The filtration was performed using Anotop 0.02 μm disposable

syringe filters from Whatman™. An argon filled glove box was used for partition experiments under conditions to exclude CO_2. Partition coefficients (mL/g) were calculated according to (1):

$$K_d = \frac{\left(\frac{A_i - A}{m}\right)}{\left(\frac{A}{V}\right)} \qquad (1)$$

Where A_i and A are the activity (cpm/mL) in the solution before and after it contacted the concrete sample, respectively; m is the mass (g) of concrete used; and V is the volume (mL) of 0.01 M NaCl or 0.01 M $NaHCO_3$ solutions containing U(VI) or Np(V).

XAFS Spectroscopy: L_{III}-edge X-ray absorption fine structure (XAFS) spectra were collected for U and Np sorption samples at the Stanford Synchrotron Radiation Laboratory (SSRL). Spectra were measured for both U and Np loaded concrete samples taken from the partition experiments over a range of pH from ~9 to12. These samples were equilibrated for ca. six months prior to XAFS measurements. In addition, "fresh" samples of U(VI) and Np(V) sorbed to treated concrete at pH 10.2 were prepared 1 month before XAFS measurement and were used as references to study potential aging effects in the actinide speciation. The samples were studied on beam line 4-1, using a Si(220) double-crystal monochromator. All spectra were collected at room temperature, either in transmission mode using argon-filled ionization chambers or in fluorescence mode using a Ge solid state detector developed at Lawrence Berkeley National Laboratory [5]. The spectra were calibrated by simultaneous measurement of UO_2 or NpO_2 references, defining the first inflection at 17166.0 eV and 17606.2 eV for the U and Np L_{III}-edges, respectively.

The XANES and EXAFS data were extracted from the raw absorption spectra by standard methods described elsewhere [6] using the suite of programs, EXAFSPAK, developed by Graham George of SSRL. Non-linear least squares curve fitting analysis was performed using EXAFSPAK to fit the raw k^3-weighted data. Modeling of the back scattering phases and amplitudes of the individual neighboring atoms was based on FEFF7.2 [7]. The input files for FEFF7.2 were prepared using the structural modeling code ATOMS 2.46b [8]. All of the modeled UO_2^{2+} and NpO_2^{+} interactions were derived from FEFF7.2 single or multiple scattering paths (SS or MS) calculated for the

model compound α-$UO_2(OH)_2$ [9]. Microsoft EXCEL™ was used to perform principal component analysis (PCA) on the spectra using standard methodology [10]. The relative contributions from the two oxidation states present in the Np L_{III} spectra were also determined empirically using the program PEAKFIT™ and data based on XANES spectra of pure Np^{4+} and NpO_2^+ standards.

Results and Discussion

1. Interaction of U(VI) with concrete

Effect of initial U concentration, concrete treatment, and dissolved carbonate -- Batch partitioning measurements of U(VI) on both untreated and treated concrete with and without added $NaHCO_3$ are shown in Figure 1a. In the absence of added $NaHCO_3$, the ambient pH of the 0.01 NaCl solutions in contact with untreated and treated concrete (under argon) were 11.21±0.13 and 10.33±0.06, respectively. By assuming equilibrium with calcite, the measured dissolved Ca concentrations were used to calculate dissolved inorganic carbon (primarily CO_3^{--}) in the 0.01 M NaCl ($3.3x10^{-5}$ and $2.4x10^{-5}$ M for the above pHs; respectively).

Figure 1a shows the partition coefficient (K_d) of U(VI), as a function of initial concentration in 0.01 M NaCl solution for treated and untreated concretes based on analysis of the unfiltered supernatants after 35 days contact under argon. Partition coefficients calculated using the analysis of the filtered supernatant were up to 4 times larger for treated concrete, but were not calculable for the untreated concrete, and at the lowest initial U concentrations for the treated concrete because supernatant concentrations were at or below the detection limit (~$2x10^{-8}$ M). K_d's for both treated and untreated concrete are large, but hydrothermal treatment reduces partitioning by

one to two orders of magnitude. Partitioning to the solid is significantly enhanced at low initial U concentrations, and appears to level off for initial U concentrations greater than ~$2x10^{-6}$ M.

The presence of carbonate in solution can reduce actinide sorption onto mineral phases due to complexation [11, 12]. In the presence of 0.01 M $NaHCO_3$ (~ 300-400 times greater dissolved carbon than in 0.01 M NaCl samples), at pH's near the ambient pH of the concrete/NaCl mixtures (10.42±0.03 and 11.21±0.08 for treated and untreated concrete, respectively), the K_d values for U(VI) are significantly lower than those in NaCl system (Figure 1a). There is little effect of concrete treatment on partitioning.

Effect of pH -- The partitioning of U(VI) vs. pH for treated concrete in 0.01 NaCl after 133 days contact is shown in Figure 2. K_d's vary by two orders of magnitude between pH 9.3 and 11.3 with a maximum between pH 10 and 11. K_d's based on analysis of filtered samples are up to an order of magnitude greater than K_d's calculated from analysis of the unfiltered samples, as previously noted for the 35 day contact-time experiments.

EXAFS – Figure 3 shows the Fourier Transformed (FT) k^3-weighted EXAFS spectra for all uranium samples. The Fourier transforms represent a pseudo-radial distribution function of the uranium near-neighbor environment, where peaks representing the near neighbor atoms appear at lower R values relative to their true distance from the U atom depending on the phase shift of the back scattering atom. Results of the non-linear least squares curve-fitting over the k-range 3-13 $Å^{-1}$ are summarized in Table 1. The uranium XAFS results show the preservation of the uranyl (UO_2^{2+}) structure in all samples. All samples also show a split equatorial shell (see Table 1).

This bond heterogeneity, as opposed to a uniform equatorial shell for the pure uranyl aquo ion, is consistent with surface adsorption and/or precipitate formation. The samples of uranium on treated concrete also showed clear evidence for a U-U interaction at 3.94 Å, suggesting that on these surfaces uranyl adsorbs or precipitates as an oligomeric species. There was no such shell observed in any of the untreated concrete samples, suggesting that uranyl forms monomeric surface complexes on the untreated concrete.

Mineral equilibrium control on U partitioning – The geochemical modeling code React (version 3.0.2; Bethke [13]) and the Lawrence Livermore National Laboratory thermodynamic data base (thermo.com.V8.R6.full (generated by GEMBOCHS.V2-Jewel.src.R6 03-dec-1996) with specific alterations and/or additions as noted; [14]), were used to assess the potential that precipitation of U-bearing phases in addition to sorption may control the concentration of uranium in solution. The GEMBOCHS thermodynamic database was modified by altering the solubility data for uranophane to that reported by Nguyen et al. [15], and including solubility data for becquerelite [16]. Analyses of solutions in contact with treated concrete for 21 to 133 days were compared to U concentrations predicted for equilibrium with a number of U-bearing phases (Figure 4a). The predicted U concentrations were calculated for equilibrium between a specific U-bearing phase and a solution with a composition defined by the measured pH and dissolved Ca and Si, and assuming that:

> Na and Cl were equal to 0.01 M plus the Na and/or Cl necessary to adjust pH above or below the ambient (10.23)
>
> Dissolved CO_2 was controlled by equilibrium with calcite at the measured pH

The system was oxidizing (fugacity O_2 = 0.2)

The measured dissolved U decreased significantly with contact time and became more dependent on pH. No single U-bearing phase equilibria could reproduce the observed U concentration vs. time and/or pH. Uranium(VI)-bearing phases such as schoepite (UO_3:$2H_2O$) and becquerelite ($Ca(UO_2)_6O_7$:$11H_2O$) are too soluble to explain the observed data; $CaUO_4$ is too insoluble. A more soluble hydrated calcium/uranium bearing phase with a stoichiometry similar to $CaUO_4$ has been suggested as a possible control on U concentrations in portlandite containing cements [17, 18]. Although thermodynamic solubility data is not available, U concentrations in the presence of this phase are on the order of 10^{-8} to 10^{-7} M; that is, in the range observed with the treated concrete samples. Equilibrium with this phase would be expected to show a pH dependence identical to crystalline $CaUO_4$, but displaced upward 2-3 orders of magnitude.

Although equilibrium with haiweeite ($Ca(UO_2)_2(Si_2O_5)_3$:$5H_2O$), soddyite ($(UO_2)_2SiO_4$:$2H_2O$), and uranophane ($Ca(UO_2)_2(SiO_3)_2(OH)_2$) predict U concentrations that overlap the observed data, these equilibria present significantly different pH dependencies. The concentration of U predicted for equilibrium with $Na_2U_2O_7$ is consistent with the 21-day data, however, the subsequent decrease in the observed dissolved U is not. It is possible that the reduction of dissolved U concentration with time will be due to the alteration of initially precipitated $Na_2U_2O_7$ to a more stable U(VI)-bearing phase. In addition to $Na_2U_2O_7$, the solubilities of two other Na/U-bearing phases (Na-weeksite -- $Na_2(UO_2)_2(Si_2O_5)_3$:$4H_2O$ and Na-boltwoodite -- $Na(H_3O)(UO_2)SiO_4$:H_2O [15]) were calculated (not shown), but were also not consistent with the observed data.

Finally, it is also possible that U may be incorporated via recrystallization [19] into the abundant calcite present in the concrete. Coprecipitation and/or solid-solution of U in calcite was not modeled. The EXAFS data for treated concrete is consistent with precipitation of any of the U(VI)-bearing phases, but does not preclude sorption and/or incorporation into calcite as partitioning mechanisms.

2. Interaction of Np(V) with concrete

Figure 1b shows the K_d's for Np(V) as a function of initial concentration of Np for untreated and treated concrete in 0.01 M NaCl and 0.01 M $NaHCO_3$. In NaCl, the K_d's for both concretes decrease with increasing initial concentration of Np(V); the K_d for untreated concrete being approximately two orders of magnitude larger than that for treated concrete. In 0.01 M $NaHCO_3$, Np(V) partitioning to both concretes is reduced, although the effect is smaller than that observed for U(VI). Figure 2 shows that the K_d for Np(V) on treated concrete is strongly pH dependent. The K_d increases monotonically by three orders of magnitude (filtered samples) in the pH range between 9.3 to 11.3.

EXAFS – The normalized Np L_{III}-edges for three representative samples (the treated pH 10.3 fresh sample, treated pH 9.3, and untreated pH 10.3 aged samples) are shown in Figure 5 along with the absorption spectra for NpO_2^+ and NpO_2 reference compounds. There is a clear time dependence in these spectra, with the fresh sample resembling NpO_2^+ and the aged samples showing a transformation to a Np^{4+}-like species. Principal Component Analysis (PCA) was performed on the sample data set and confirmed the presence of two components. Target testing

was performed on four spectra representing the 3+, 4+, 5+, and 6+ oxidation states. A positive fit was found for the Np^{4+} and NpO_2^+ models while a negative fit was found for the Np^{3+} and NpO_2^{2+} models. The percentage of NpO_2^+ in the samples was subsequently determined using the software PEAKFIT™ and reference spectra for the pure Np^{4+} and NpO_2^+ components.

Table 2 gives the results of the EXAFS curve fitting for all samples along with the % NpO_2^+ for each sample as determined by EXAFS and XANES. The EXAFS data extended out to k=9 $Å^{-1}$, which limits the ability to resolve equatorial oxygens bonded to NpO_2^+ (R=2.3-2.5 Å) from oxygens bonded to Np^{4+} (R~2.4 Å). As a result, the % NpO_2^+ was determined by varying the axial oxygen coordination number, N_{Oax} (i.e., N_{Oax}=2 for 100% NpO_2^+). The freshly prepared sample of Np at pH=10.3 on treated concrete is observed to have the highest amount of NpO_2^+ at ~78%. The other Np samples aged for ~6 months in contact with treated and untreated concrete are all observed to have NpO_2^+ fractions between 36-60%. Although the fraction of Np(IV) associated with the concrete increased over time, neither the XANES nor the EXAFS spectra show the characteristic features attributable to solid-phase NpO_2.

Mineral equilibrium control on Np partitioning – In contrast to U, the concentration of dissolved Np decreased only slightly, or remained nearly constant, in contact with treated concrete over the period from 21 to 133 days (Figure 4b). In an attempt to explain the observed Np concentrations by solid phase equilibria, the GEMBOCHS data base was modified and/or augmented by including solubility data for $NpO_2OH(am)$ [20], $Np_2O_5(c)$ [21, 22], and $Np(IV)O_2$ [23]. The solubility was calculated initially (solid lines) by considering only a single hydrolysis species of Np(V) ($NpO_2OH^o_{aq}$, $\log \beta_1 = 5.1$; [23]). The solubilities of $Np_2O_5(c)$ and NpO_2 were also calculated

(dotted lines) considering a less stable first hydrolysis constant of NpO_2^+ (log β_1 = 2.7; [24]) as well as a second hydrolysis species ($NpO_2(OH)^-_2$, log β_2 = 4.35; [24]). As figure 4b shows, Np(V)- and Np(IV)-bearing oxides and hydroxides cannot explain the observed trend in Np vs. pH. Although by decreasing the stability of the first hydrolysis constant of NpO_2^+, it is possible to simulate the decrease in Np concentration with increasing pH, the slope of the simulated decrease is too small to explain the measurements. Neptunium(V) carbonate phases were also considered, but were found to be orders of magnitude too soluble to explain the observed data. We conclude that sorption of Np(V) controls the partitioning between treated concrete and liquid, and that the observed reduction of sorbed Np(V) to Np(IV) does not appreciably affect this distribution, nor does it apparently result in the precipitation of NpO_2. Although the site of Np sorption on the treated concrete cannot be identified, previous work has shown that calcite is an effective sorbent for Np(V) [25].

3. Colloid-associated U and Np

As noted above, K_d's based on analysis of the unfiltered supernatants were always smaller than those calculated from filtered samples and suggests that a significant fraction of U and Np were associated with the filterable particles. Comparison of U and Np concentrations in unfiltered and filtered supernatants for the 0.01 NaCl samples show that for untreated concrete, nearly 100% of U and Np were associated with particulates, and for treated concrete, approximately 80% of Np was associated with the filtered colloids. Clearly, the concentration of suspended colloids in these experiments is large because of the crushing required to reduce the particle size to < 53 μm. The concentration of suspended colloids would be expected to be much smaller for fluids inter-

acting with intact concrete. The partitioning of U and Np based on the unfiltered supernatants thus provides a minimum measure of U and Np retardation.

The total U and Np concentrations (colloidal + soluble) are observed to decrease over time, most likely due to coagulation and settling of the actinide-bearing concrete colloids. Therefore, the 'apparent' K_d as calculated based on analysis of the unfiltered samples increases with time. Thus, the 'apparent' K_d based on unfiltered samples after short contact times provides a 'conservative' measure of the ability of the concrete to retard U(VI) and Np(V).

The fraction of U and Np associated with colloids was reduced in the 0.01 M $NaHCO_3$/concrete experiments. Our results show that no detectable U-bearing concrete colloids were observed in 0.01 M $NaHCO_3$ solution with both untreated and treated concrete. For Np in 0.01 M $NaHCO_3$, ca. 72% and 30% are associated with suspended particles for untreated and treated concrete, respectively.

In a related study of Np and U transport through hydrothermally altered concrete, colloids generated from the treated concrete via crushing and ultrasonic treatment (median size ~ 0.3 μm) were analyzed by X-ray diffraction and found to consist primarily of calcite and smectite [26]. ICP-AES analysis of the unfiltered supernatants for treated concretes is consistent with this mineralogy; that is, they have higher silica and calcium concentrations than the filtered samples.

Conclusions

Both treated and untreated concrete show strong partitioning of U(VI) and Np(V) to the solid in the pH range 9 to 11.5. However, hydrothermal treatment significantly reduced the partitioning

for both U and Np. The decrease in partitioning due to hydrothermal treatment may result from mineralogical (e.g., conversion of poorly crystalline phases and portlandite to crystalline calcium silicate hydrate phases), chemical (in particular, the significant decrease in pH), and/or physical changes (e.g., potential decrease in specific surface area) attendant to the hydrothermal treatment. Dissolved carbonate reduces the partitioning of both nuclides, on both concretes, but a larger impact was observed for U(VI). The partitioning is strongly pH dependent for both nuclides. For U, partitioning to the treated concrete may be controlled by precipitation of U(VI) bearing phases, for Np, sorption appears to be the dominant process controlling partitioning. Sorbed Np(V) is reduced to Np(IV) during contact with both treated and untreated concrete. Strong partitioning to the solid phase, together with the presence of colloids generated by the sample treatment, resulted in a major fraction of U and Np in the supernatant associated with the suspended particles in the 0.01 M NaCl samples. Partition coefficients based on analysis of unfiltered samples provide a conservative estimate for U and Np retardation through concrete, however, because of the large K_d's, there is a potential for colloid-enhanced transport.

Acknowledgements

This work was performed under the auspices of the U.S. Department of Energy by Lawrence Livermore National Laboratory under Contract W-7405-Eng-48. This work was partly supported by the Yucca Mountain Site Characterization Project at LLNL. This work was done (partially) at SSRL, which is operated by the Department of Energy, Division of Chemical Sciences. Additional XAFS experimental support was provided by D. Caulder and W. Lukens and the Actinide Chemistry Group at Lawrence Berkeley National Laboratory.

References

1. M. Atkins, F. P. Glasser, Mat. Res. Soc. Symp. Proc. (1990).

2. T. G. Heath, D. J. Ilett, C. J. Tweed, Mat. Res. Soc. Symp. Proc. (1996).

3. B. F. Greenfield, D. J. Ilett, M. Ito, R. McCrohon, T. G. Heath, C. J. Tweed, S. J. Williams, M. Yui, *Radiochimica Acta* **82**, 27-32 (1998).

4. J. D. F. Ramsay, R. G. Avery, P. J. Russell, *Radiochimica Acta* **44-5**, 119-124 (1988).

5. J. J. Bucher, N. M. Edelstein, K. P. Osborne, D. K. Shuh, N. Madden, P. Luke, D. Pehl, C. Cork, D. Malone, P. G. Allen, *Reviews Scientific Instruments* **67** (1996).

6. R. Prins, D. E. Koningsberger, Eds., *X-Ray* Absorption*: Principles, Applications, Techniques for EXAFS, SEXAFS, and XANES* (Wiley-Interscience, 1988).

7. J. Mustre de Leon, J. J. Rehr, S. Zabinsky, R. C. Albers, Physical *Review B* **44**, 4146-4156 (1991).

8. B. Ravel, "ATOMS, a program to generate atom lists for XAFS analysis from crystallographic data." (University of Washington, Seattle, WA., 1996).

9. J. C. Taylor, H. J. Hurst, *Acta Cryst. B* **27**, 2018-2022 (1971).

10. E. R. Malinowski, *Factor Analysis in Chemistry* (Wiley-Interscience, 1991).

11. M. Del Nero, K. Ben Said, A. Clement, G. Bontems, *Radiochimica Acta* **81**, 133-141 (1998).

12. K. H. Lieser, S. Quandtklenk, B. Thybusch, *Radiochimica Acta* **57**, 45-50 (1992).

13. C. M. Bethke, *The Geochemists Workbench,* Release *3.0, A Users Guide to Rxn, Act2, Tact, React, and Gtplot* (Copyright Craig M. Bethke, Hydrogeology Program, University of Illinois, Champaign, IL., 1998).

14. J. Johnson, S. Lundeen, "GEMBOCHS Thermodynamic Datafiles For Use With the EQ3/6 Software Package" *Yucca Mountain* Project *Milestone Report M0L72.* (Lawrence Livermore National Laboratory, 1994).

15. S. N. Nguyen, R. J. Silva, H. C. Weed, J. E. Andrews, *Journal of Chemical Thermodynamics* **24**, 359 (1992).

16. M. C. A. Sandino, B. Grambow, *Radiochimica Acta* **66**, 37 (1994).

17. M. Atkins, F. P. Glasser, L. P. Moroni, The long-term properties of cement and concretes, Mat. Res. Soc. Symp. Proc. (1991).

18. L. P. Moroni, G. F.P., *Waste* Management **15**, 243-254 (1995).

19. D. E. Meece, L. K. Benninger, Geochimica *et Cosmochimica Acta* **57**, 1447-1458 (1993).

20. K. E. Roberts, H. B. Silber, P. C. Torretto, T. Prussin, K. Becraft, D. E. Hobart, C. F. Novak, *Radiochimica Acta* **74**, 27-30 (1996).

21. P. J. Pan, A. B. Campbell, *Radiochimica Acta* 81, 73 (1998).

22. D. W. Efurd, W. Runde, J. C. Banar, D. R. Janecky, J. P. Kaszuba, P. D. Palmer, F. R. Roensch, C. D. Tait, *Environmental Science & Technology* **32**, 3893 (1998).

23. R. J. Lemire, "An assessment of the thermodynamic behavior of neptunium in water and model groundwater from 25 to 150 deg C" *AECL-7817* (Atomic Energy of Canada Limited, 1984).

24. V. Neck, J. I. Kim, B. Kanellakopulos, Radiochimica *Acta* **56**, 25 (1992).

25. W. L. Keeney-Kennicutt, J. W. Morse, *Marine* Chemistry **15**, 133-150 (1984).

26. S. L. Matzen, J. M. Beiriger, P. C. Torretto, P. Zhao, B. E. Viani, *Radiochimica Acta* **this volume**.

Table 1. EXAFS best least-squares fitting results for the uranium samples.

Sample	Shell	N[a]	R (Å)[a]	σ^2 (Å^2)[b]
Treated concrete, pH 9.3	U-O_{ax}	2.00	1.81	0.00201
	U-O_{eq1}	4.33	2.30	0.00776
	U-O_{eq2}	1.82	2.48	0.00776
	U-U	0.64	3.96	0.00076
Treated concrete, pH 10.3	U-O_{ax}	2.00	1.82	0.00115
	U-O_{eq1}	3.38	2.28	0.00606
	U-O_{eq2}	2.22	2.44	0.00606
	U-U	1.07	3.96	0.00338
Treated concrete, pH 11.3	U-O_{ax}	2.00	1.81	0.00268
	U-O_{eq1}	2.90	2.26	0.00330
	U-O_{eq2}	2.16	2.42	0.00330
	U-U	1.51	3.96	0.00603
Untreated concrete, pH 10.3	U-O_{ax}	2.00	1.82	0.00184
	U-O_{eq1}	3.33	2.28	0.00687
	U-O_{eq2}	1.70	2.45	0.00687
Untreated concrete, pH 11.3	U-O_{ax}	2.00	1.83	0.00242
	U-O_{eq1}	4.56	2.29	0.00967
	U-O_{eq2}	1.36	2.53	0.00967
Untreated concrete, pH 12.3	U-O_{ax}	2.00	1.83	0.00216
	U-O_{eq1}	2.54	2.23	0.00163
	U-O_{eq2}	1.44	2.39	0.00163
Fresh[c], treated concrete, pH 10.3	U-O_{ax}	2.00	1.81	0.00255
	U-O_{eq1}	3.40	2.30	0.00418
	U-O_{eq2}	1.69	2.49	0.00418

[a]The 95% confidence limits for the bond lengths (R) and coordination numbers (N) for each shell are: U-O_{ax}: ±0.001 Å; U-O_{eq1}: ±0.003 Å and ±0.3; U-O_{eq2}: ±0.01 Å and ±0.2; U-$U_{(1-3)}$: ±0.005 Å and ±0.3, respectively.

[b]σ is the EXAFS Debye-Waller term that accounts for the effects of thermal and static disorder through damping of the EXAFS oscillations by the factor $\exp(-2k^2\sigma^2)$.

[c]Fresh signifies U/concrete contact time ~1 month; for other samples U/concrete contact time ~6 months.

Table 2. EXAFS best least-squares fitting results and % NpO_2^+ determination for the neptunium samples at the L3 edge.

Sample	Shell	N[a]	R (Å)[a]	σ^2 (Å^2)[b]	% by XANES fit[c]	% by Np-O_{axial} fraction[c]
Treated concrete, pH 9.3	Np-O_{axial}	0.896	1.82	0.00300	36.3	45.0
	Np-O	4.43	2.39	0.00915		
Treated concrete, pH 10.3	Np-O_{axial}	1.24	1.86	0.00300	47.6	62.0
	Np-O	5.65	2.39	0.01535		
Treated concrete, pH 11.3	Np-O_{axial}	0.850	1.85	0.00300	44.9	43.0
	Np-O	4.24	2.39	0.00971		
Untreated concrete, pH 10.3	Np-O_{axial}	0.709	1.84	0.00300	37.8	36.0
	Np-O	4.55	2.38	0.00940		
Untreated concrete, pH 11.3	Np-O_{axial}	0.736	1.84	0.00300	38.8	37.0
	Np-O	4.66	2.40	0.00902		
Untreated concrete, pH 12.3	Np-O_{axial}	1.00	1.86	0.00300	45.9	50.0
	Np-O	3.35	2.39	0.00421		
Fresh[d], treated concrete, pH 10.3	Np-O_{axial}	1.56	1.86	0.00300	78.9	77.0
	Np-O	3.39	2.44	0.00792		

[a]The 95% confidence limits for the bond lengths (R) and coordination numbers (N) for each shell are: Np-O_{axial}: ±0.004 Å and ±0.05; Np-O_{oxide}: ±0.003 Å and ±0.3, respectively.

[b]σ is the EXAFS Debye-Waller term that accounts for the effects of thermal and static disorder through damping of the EXAFS oscillations by the factor $\exp(-2k^2\sigma^2)$.

[c]The 95% confidence limits for % Np(V) are ±2.5% for determination by EXAFS Np-O_{axial} fraction and ±7% for determination by XANES component fitting.

[d]Fresh signifies Np/concrete contact time ~1 month; for other samples Np/concrete contact time ~6 months.

FIGURE CAPTIONS

Figure 1. Partition coefficients (K_d's) for (a) U and (b) Np on untreated and hydrothermally altered (treated) concretes. K_d's are calculated based on analysis of unfiltered supernatants. Error bars represent uncertainty in counting statistics only.

Figure 2. Partition coefficients (K_d) for U (8.05×10^{-6} M) and Np (1.09×10^{-5} M) onto hydrothermally altered concrete vs. pH after 133 days. Error bars represent uncertainty in counting statistics only.

Figure 3. Fourier transforms of U L_{III} EXAFS for (a) freshly prepared U on treated concrete, pH 10.3, (b) U on treated concrete, pH 12.3, (c) U on treated concrete, pH 11.3, (d) U on treated concrete, pH 10.3, (e) U on untreated concrete, pH 11.3, (f) U on untreated concrete, pH 10.3, and (g) U on untreated concrete, pH 9.3. Fresh signifies U/concrete contact time = ~1 month; for other samples U/concrete contact times = ~6 months. The dashed line is the experimental data, and the solid line corresponds to the best theoretical fit to the data.

Figure 4. Comparison of measured (a) U and (b) Np solution concentrations with predictions based on equilibrium with U- and Np-bearing phases. See text for discussion of thermodynamic data used for model predictions.

Figure 5. Normalized Np L_{III} XANES for (a) aqueous Np(V) reference, NpO_2^+, (b) freshly prepared Np on treated concrete, pH 10.3, (c) Np on untreated concrete, pH 10.3, (d) Np on treated concrete, pH 9.3, and (e) Np(IV) oxide reference, NpO_2. Fresh signifies Np/concrete contact time = ~1 month; for other samples Np/concrete contact times = ~6 months.

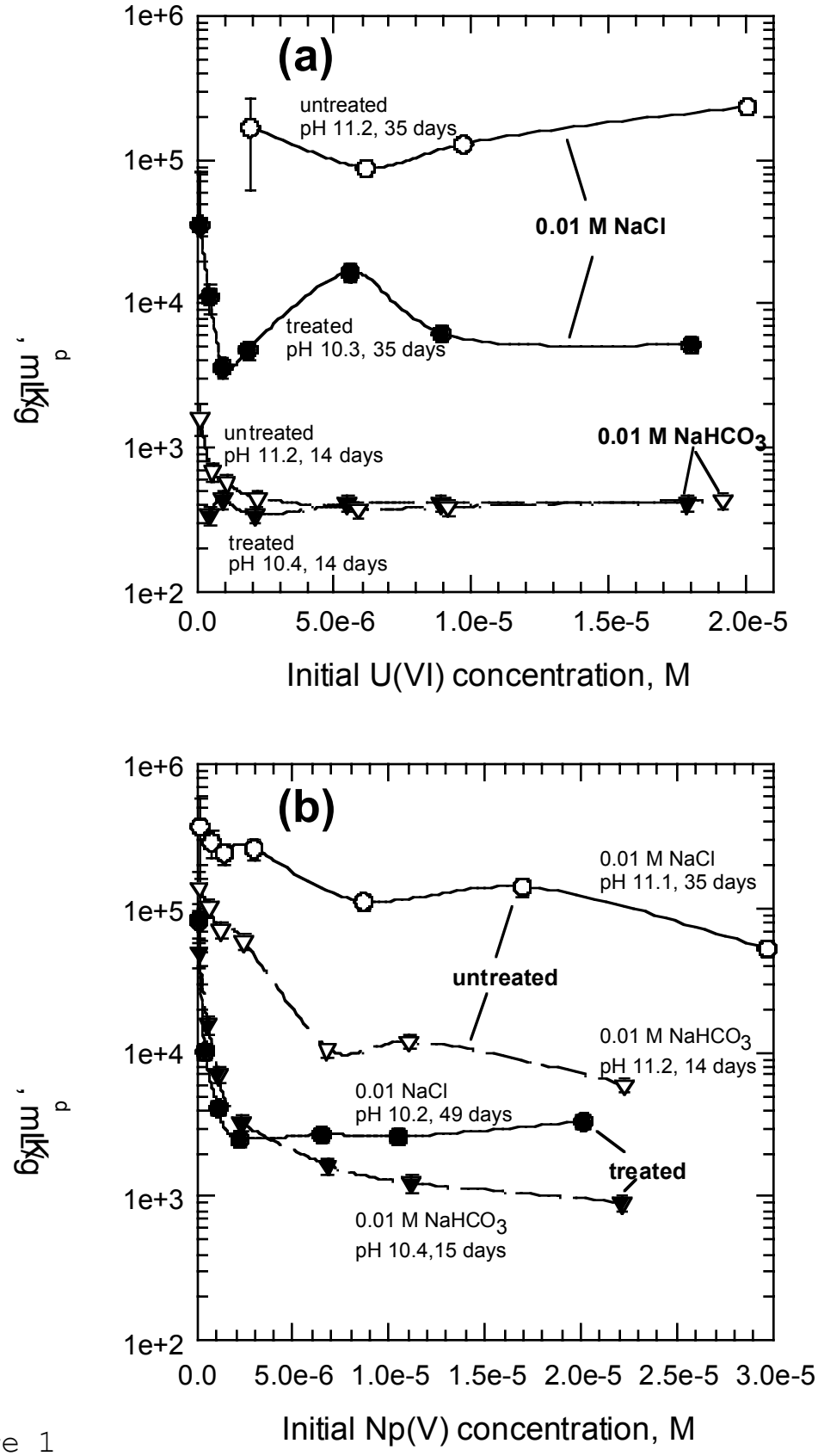
(a)
untreated
pH 11.2, 35 days
0.01 M NaCl
treated
pH 10.3, 35 days
untreated
pH 11.2, 14 days
0.01 M NaHCO3
treated
pH 10.4, 14 days
1e+6
1e+5
1e+4
1e+3
1e+2
0.0
5.0e-6
1.0e-5
1.5e-5
2.0e-5
Initial U(VI) concentration, M
(b)
0.01 M NaCl
pH 11.1, 35 days
untreated
0.01 M NaHCO3
pH 11.2, 14 days
0.01 NaCl
pH 10.2, 49 days
treated
0.01 M NaHCO3
pH 10.4,15 days
1e+6
1e+5
1e+4
1e+3
1e+2
0.0
5.0e-6
1.0e-5
1.5e-5
2.0e-5
2.5e-5
3.0e-5
Initial Np(V) concentration, M

Figure 1

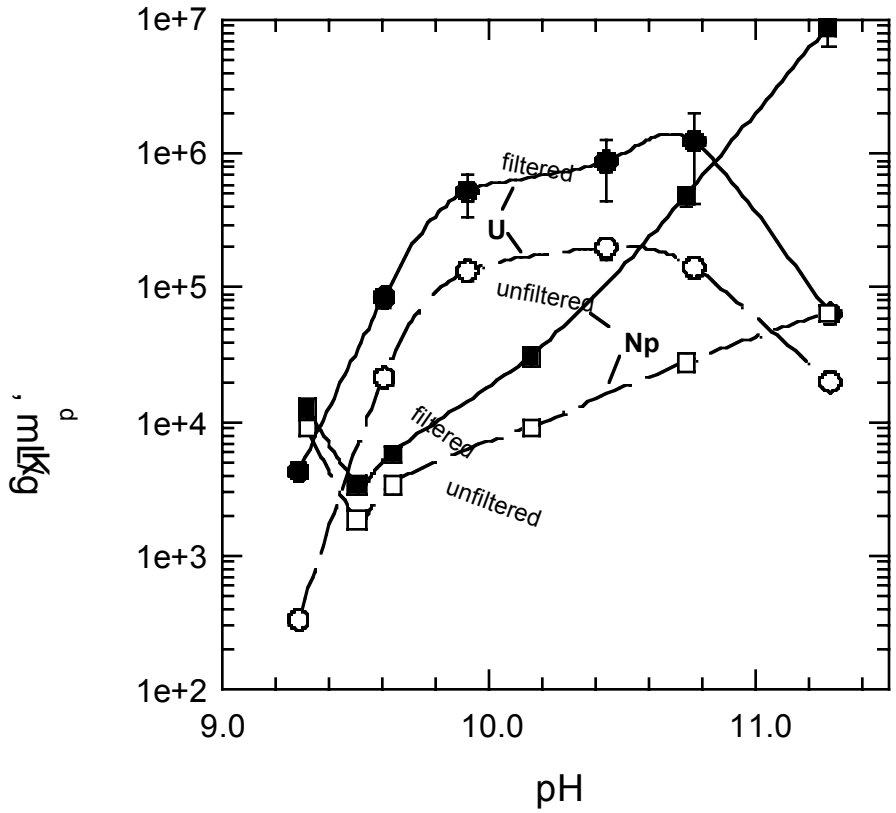
1e+7
1e+6
1e+5
1e+4
1e+3
1e+2
9.0
10.0
11.0
pH
K_d, mL/g
filtered
U
unfiltered
Np
filtered
unfiltered

Figure 2

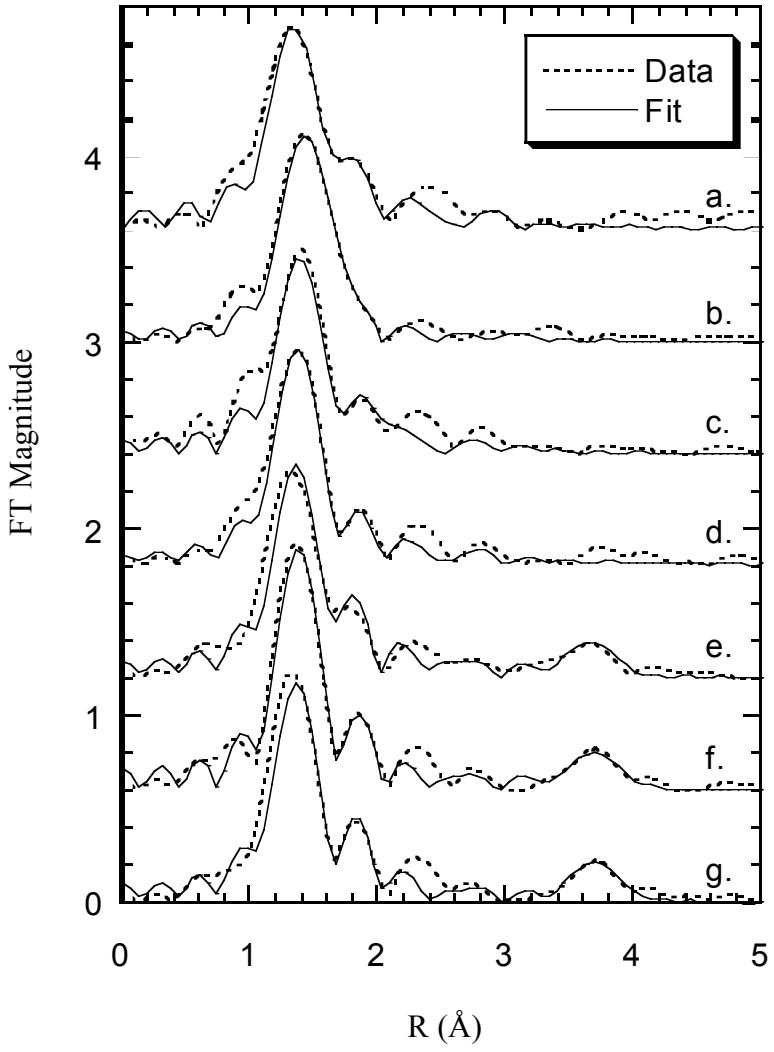

Figure 3

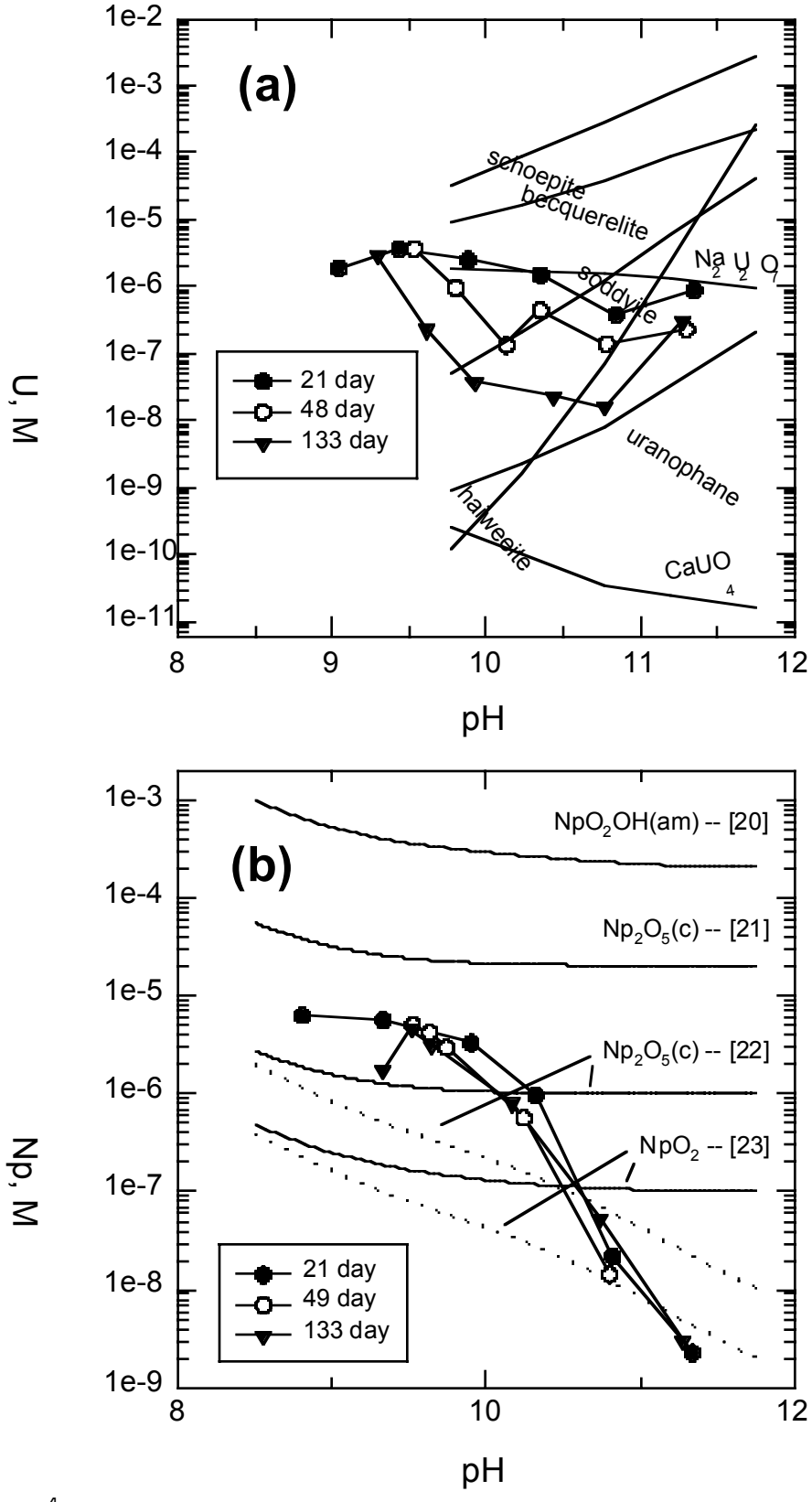
(a)
schoepite
becquerelite
soddyite
uranophane
haiweeite
21 day
48 day
133 day
U, M
pH
(b)
NpO2OH(am) -- [20]
Np2O5(c) -- [21]
Np2O5(c) -- [22]
NpO2 -- [23]
21 day
49 day
133 day
Np, M
pH

Figure 4

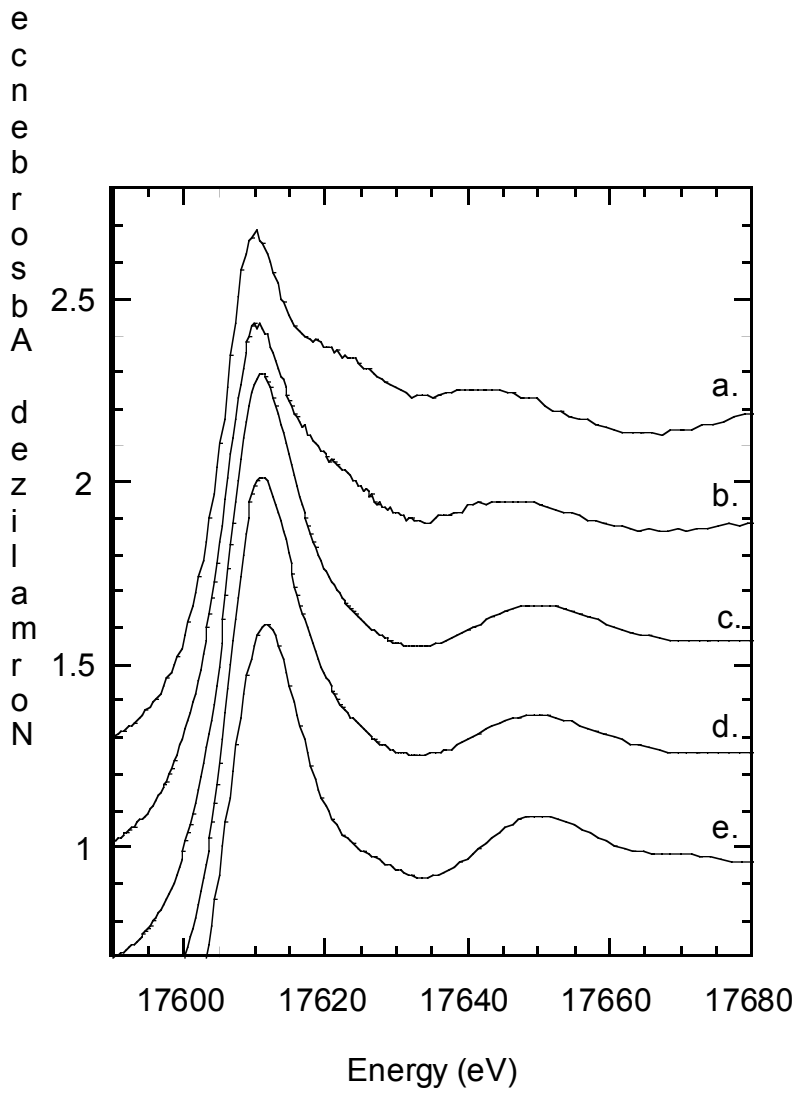
Absorbance
2.5
2
1.5
1
a.
b.
c.
d.
e.
17600
17620
17640
17660
17680
Energy (eV)

Figure 5